Tracking Error Analysis for Feedback Systems With Hysteresis Inversion and Fast Linear Dynamics[1]

Mohamed Edardar
Electrical and Electronic Engineering,
University of Tripoli,
Tripoli, Libya
e-mail: moh_edardar@yahoo.com

Xiaobo Tan
Electrical and Computer Engineering,
Michigan State University,
428 S. Shaw Lane,
East Lansing, MI 48824
e-mail: xbtan@egr.msu.edu

Hassan K. Khalil
Electrical and Computer Engineering,
Michigan State University,
428 S. Shaw Lane,
East Lansing, MI 48824
e-mail: khalil@egr.msu.edu

Analysis of closed-loop systems involving hysteresis is important to both the understanding of these systems and the synthesis of control schemes. However, such analysis is challenging due to the nonsmooth nature of hysteresis nonlinearities. In this paper, singular perturbation techniques are employed to derive an analytical approximation to the tracking error for a system consisting of fast linear dynamics preceded by a piecewise linear hysteresis nonlinearity, which is motivated by applications such as piezo-actuated nanopositioning. The control architecture considered combines hysteresis inversion and proportional-integral feedback, with and without a constant feedforward control. The analysis incorporates the effect of uncertainty in the hysteresis model, and offers insight into how the tracking performance depends on the system parameters and the references, thereby offering guidance in the controller design. Simulation and experimental results on a piezo-actuated nanopositioning system are presented to support the analysis. In particular, the control scheme incorporating the feedforward element consistently outperforms the classical PI controller in tracking a variety of references.
[DOI: 10.1115/1.4026511]

1 Introduction

Hysteresis is a nonlinear phenomenon that exists in various areas, such as smart materials, biology, geology, mechanics, and economics, and it presents challenges in both the understanding and control of such systems. Modeling, analysis, and control of systems with hysteresis have received great attention over the last two decades. For example, piezoelectric actuators are commonly used in nanopositioning applications such as scanning tunneling microscopy and atomic force microscopy. They have large bandwidth and can produce large mechanical forces [1,2], but their hysteretic behavior has been a major challenge in achieving high-speed precision control [1].

The control methods dealing with hysteresis can be roughly classified into open-loop inverse compensation methods and methods involving feedback. Open-loop inverse control [3–7] can result in small tracking errors, but it typically only applies in the case where system dynamics (other than hysteresis) are ignored, and is susceptible to model uncertainties and environmental changes. Therefore, a popular approach in coping with hysteresis is to construct an inverse operator and integrate it with feedback techniques [7–14]. These feedback control schemes can include, for example, proportional-integral-derivative control, adaptive control [7,10,12,13,15], robust control [11,16,17], and robust-adaptive control [18–20].

A main concern for feedback methods is stability. Stability analysis for hysteretic systems involving adaptation is presented in Refs. [7,10,12,13] under various persistent-excitation-type conditions on the reference signals. Robust control methods for hysteresis control include for example servo-compensators [14] and sliding-mode controllers [16,17]. In these methods, researchers avoid the complex adaptation algorithms and typically assume that a bound on the inversion error is known to establish the stability of the closed-loop system. There are also schemes that do not fall into aforementioned categories. For example, in Ref. [21] Valadkhan et al. establish bounded-input-bounded-output stability for a proportional-integral controlled hysteresis operator (without system dynamics). Wu and Zou established asymptotic convergence in tracking a periodic signal under an iterative learning control, and used the latter scheme to compensate for hysteresis and vibrational dynamics in piezo actuators [22]. Ge and Jouaneh proposed a feedforward inverse scheme in combination with a proportional integral differential controller [23] for a piezo actuator, which was proven effective experimentally without stability analysis. In summary, despite the significant body of work on analysis of systems with hysteresis, derivation of an analytical approximation for the closed-loop tracking error in terms of system parameters has not been reported.

The contributions of this paper are twofold. The first contribution is a novel singular perturbation analysis method for understanding the closed-loop behavior of systems with hysteresis and fast linear dynamics. The second contribution is the proposal of a modified PI controller, where a constant feedforward term is included, for the class of systems under consideration, and demonstration of the effectiveness of such a strategy through analysis, simulation, and experimentation. While the second contribution is of clear engineering interest, we note that the first contribution is also well motivated by engineering applications. In particular, the presented analysis approach sheds light on how hysteresis parameters, uncertainties, and control gains interact in the closed-loop system and determine the size of the tracking error, and consequently, it provides insight and guidance for the design of controller gains. For example, the analysis reveals how the tracking error scales with the reference frequency, a question of practical interest but remaining largely open until now. A more detailed account of the contributions follows.

Motivated by the properties of piezo-actuated nanopositioning systems, we assume that the linear dynamics of the plant are

[1]The work was supported by the National Science Foundation (CMMI 0824830, CMMI 1301243).

Contributed by the Dynamic Systems Division of ASME for publication in the Journal of Dynamic Systems, Measurement, and Control. Manuscript received November 20, 2012; final manuscript received December 27, 2013; published online April 4, 2014. Assoc. Editor: Qingze Zou.

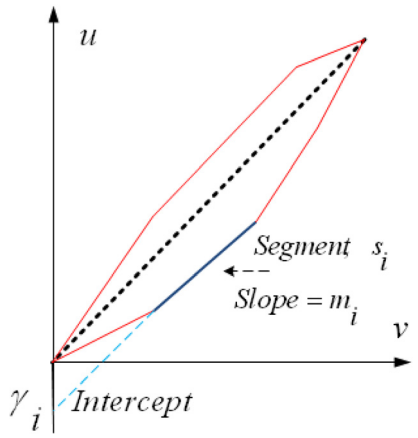

Fig. 1 Illustration of a hysteresis loop with piecewise linear characteristics

stable and have large bandwidth. This assumption allows us to use singular perturbation techniques to separate the slow dynamics of the controller from the fast dynamics of the plant and obtain an explicit expression for the tracking error, where we can discuss the effect of different parameters on the size of the error. In addition, we assume that the hysteresis nonlinearity has piecewise linear characteristics; in other words, all hysteresis loops (major loops and minor loops) consist of linear segments, where each segment s_i has a slope m_i and an intercept γ_i with the vertical axis. See Fig. 1 for illustration. The tracking error analysis is conducted for a control scheme that combines the hysteresis inversion with proportional-integral feedback controller and a constant-gain feedforward term as illustrated in Fig. 2. Although the case without the feedforward component has been reported extensively in the literature [9,10,12–17], we show in this paper the advantage of adding a feedforward gain component. We note that feedforward control has been discussed in tracking problems with two-degree-of-freedom control [24–27] and proved to be useful in performance improvement, but its combination with feedback and inversion for systems with hysteresis has not been reported before.

The analysis in this work is a continuation of our work presented in Ref. [28]. The previous work [28], was limited to the analysis of the driving terms of the tracking error when the hysteresis is on a particular linear segment. As such, it did not provide insight into the cumulative behavior when the hysteresis traverses different linear segments, as well as the frequency-scaling behavior that is presented in the current work.

With nanopositioning control as an example, extensive simulation and experimental results are presented to support the proposed analysis approach and the modified PI control scheme. In particular, the comparison on the frequency-scaling behavior of the tracking error is provided between the simulation results and the analytical bound, where good agreement is achieved. Experimental results on tracking a variety of references, including sinusoids, multisine signals, and sawtooth signals, demonstrate that the PI controller with the feedforward component outperforms the classical PI controller consistently.

The remainder of the paper is organized as follows. In Sec. 2, we briefly describe the closed-loop system. This is followed by the derivation of an explicit expression for the tracking error in Sec. 3. Tracking error analysis is provided in this section by studying the system model using singular perturbation approximation. Moreover, a bound on the propagating error is derived, and the frequency-scaling analysis is provided. Simulation and experimental results are presented in Sec. 4. Finally, we provide concluding remarks in Sec. 5.

2 Closed-Loop System Setup

In this section, we briefly describe the components of the closed-loop system as illustrated in Fig. 3. The linear dynamics of the plant are represented by a singularly perturbed system. The bandwidth of the dynamics ω_n is assumed to be large and of the order $1/\varepsilon$, where ε is a small positive parameter. The model of the linear plant is given by

$$\begin{aligned} \varepsilon \dot{z} &= Az + Bu, \\ y &= Cz \end{aligned} \tag{1}$$

where A is a Hurwitz matrix, B and C are matrices with proper dimensions, and z is the state vector. We assume that the feedback controller is a proportional-integral controller, represented as

$$\begin{aligned} \dot{x} &= e = y_r - y = y_r - Cz, \\ w &= k_i x + k_p e \end{aligned} \tag{2}$$

where e is the tracking error and w is the output of the proportional-integral controller. A feedforward path with a gain g is used to compensate for the DC gain of the linear dynamics. When $g = 0$, the scheme falls back into the one scheme that combines hysteresis inversion (in the feedback loop) and feedback control.

We denote the hysteresis operator by Γ_p and the inverse operator as Γ_m^{-1}. The input-output relationship of Γ_p can be described in each segment of a hysteresis loop as follows:

$$u = m_i v + \gamma_i \tag{3}$$

The DC gain of the plant is

$$h = -CA^{-1}B \tag{4}$$

The input to the inverse operator, u_d, and its output, v, are expressed as[2]

$$u_d = g y_r + k_i x + k_p e \tag{5}$$

$$v = \frac{1}{m}(u_d - \gamma) \tag{6}$$

Note that Eq. (6) is essentially the inversion process for the piecewise linear hysteresis model, and it requires tracking which linear segment the hysteresis characteristic is on at each time instant. Such an assumption is standard in hysteresis inversion since the past history of v is available. We further note that Eq. (6) requires knowing the slope and intercept of the current linear segment; when such knowledge is not precise, we can represent it as follows. Let us denote the corresponding slope of the plant hysteresis Γ_p by m_p and the intercept by γ_p with parameter uncertainties Δ_m and Δ_γ, where $m_p = m + \Delta_m$ and $\gamma_p = \gamma + \Delta_\gamma$, which implies

$$u = (m + \Delta_m)v + (\gamma + \Delta_\gamma) \tag{7}$$

By substituting u_d from Eq. (5) and v from Eq. (6) into Eq. (7), we express u as

$$u = \frac{m + \Delta_m}{m}[g y_r + k_i x + k_p(y_r - Cz)] + \frac{m\Delta_\gamma - \gamma\Delta_m}{m} \tag{8}$$

The singularly perturbed closed-loop system, obtained by inserting u from Eq. (8) into Eq. (1), is given by

[2]For convenience, we will drop the subscript i in the analysis unless necessary and use m and γ to denote the slope and intercept of the line segment under consideration.

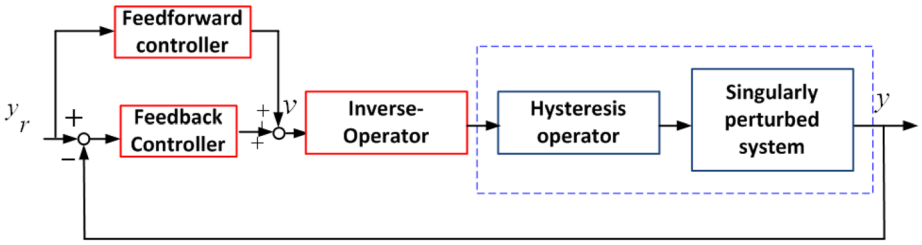

Fig. 2 The proposed scheme for singularly perturbed systems preceded by hysteresis with added feedforward branch

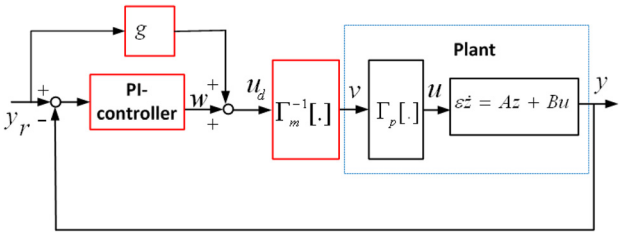

Fig. 3 Hysteresis inverse in the feedback path

$$\begin{aligned}\dot{x} &= y_r - Cz\\ \varepsilon\dot{z} &= \left[A - \frac{k_p(m+\Delta_m)}{m}BC\right]z + B\frac{m+\Delta_m}{m}(g+k_p)y_r\\ &\quad + B\frac{m+\Delta_m}{m}k_i x + B\left(\frac{m\Delta_\gamma - \gamma\Delta_m}{m}\right)\end{aligned} \tag{9}$$

3 Tracking Error Analysis

In order to get a rough idea of what factors determine the size of the error, we first assume in Sec. 3.1 that the plant is represented by a DC gain (i.e., it has an infinite bandwidth). This is equivalent to setting $\varepsilon = 0$. In this case, the tracking error e is captured by the slow model alone. We focus here on showing how the tracking error is affected by the input reference. Then, in the following subsections we discuss other factors that determine the size of the tracking error by solving the closed-loop system equations with periodic references.

3.1 Analysis Using the Slow Model Approximation. For the fast model of the singularly perturbed system to be exponentially stable, we assume that the matrix $[A - (k_p(m+\Delta_m)/m)BC]$ of Eq. (9) is Hurwitz. To obtain an approximation of the slow model, we set $\varepsilon = 0$, to get

$$\begin{aligned}z = -\left[A - \frac{k_p(m+\Delta_m)}{m}BC\right]^{-1} B\left[\frac{m+\Delta_m}{m}(g+k_p)y_r\right.\\ \left. + \frac{m+\Delta_m}{m}k_i x + \left(\frac{m\Delta_\gamma - \gamma\Delta_m}{m}\right)\right]\end{aligned} \tag{10}$$

We insert z from Eq. (10) into the $\dot{x}$-equation (9) and use the matrix inversion lemma [29], to obtain the approximate slow model as

$$\begin{aligned}\dot{x} &= \frac{-(m+\Delta_m)hk_i}{m+k_p(m+\Delta_m)h}x + \frac{m(1-gh)-\Delta_m gh}{m+k_p(m+\Delta_m)h}y_r\\ &\quad - h\frac{m\Delta_\gamma - \gamma\Delta_m}{m+k_p(m+\Delta_m)h}\end{aligned} \tag{11}$$

Equation (11) motivates the choice of $g = 1/h$. This would reduce the error due to the y_r term, and $\dot{x}$ becomes

$$\begin{aligned}\dot{x} &= \frac{-(m+\Delta_m)hk_i}{m+k_p(m+\Delta_m)h}x + \frac{-\Delta_m}{m+k_p(m+\Delta_m)h}y_r\\ &\quad - h\frac{m\Delta_\gamma - \gamma\Delta_m}{m+k_p(m+\Delta_m)h}\end{aligned} \tag{12}$$

When the feedforward path is not included, we set $g = 0$ in Eq. (11) and obtain

$$\begin{aligned}\dot{x} &= \frac{-(m+\Delta_m)hk_i}{m+k_p(m+\Delta_m)h}x + \frac{m}{m+k_p(m+\Delta_m)h}y_r\\ &\quad + h\frac{m\Delta_\gamma - \gamma\Delta_m}{m+k_p(m+\Delta_m)h}\end{aligned} \tag{13}$$

To have a general idea from this approximation about the steady-state tracking error, here we only discuss the second term on the right-hand side of Eqs. (12) and (13), which determines the contribution of the reference signal y_r to the tracking error e (i.e., $\dot{x}$). By comparing Eqs. (12) and (13) we notice that when Δ_m is small compared to the slope m, the tracking error e will be less influenced by y_r when feedforward is used. Moreover, in the ideal case $(\Delta_m = 0 = \Delta_\gamma)$, the tracking error becomes independent of the reference signal y_r. In this case, the solution of the differential equation will only have a decaying transient term dependent on the initial value of x but independent of the segment's slope m, and according to singular perturbation theory [30] the full solution x is $O(\varepsilon)$ to the solution of Eq. (12); that is,

$$x(t) = x(0)e^{-\frac{k_i h}{1+k_p h}t} + O(\varepsilon) \tag{14}$$

The effect of the linear dynamics which are ignored in the low-frequency approximation, is abstracted in the term $O(\varepsilon)$. It is important to consider this term at high frequencies as we will see in later analysis. From Eqs. (12) and (13), one can say that by increasing the gain k_p the error would decrease. However, k_p might be constrained by the stability of the system because, for high-order linear dynamics, increasing the gain k_p beyond a certain value may destabilize the closed-loop matrix $[A - (k_p(m+\Delta_m)/m)BC]$. It is also important to have the ratio k_i/k_p high in order to achieve fast decay in Eq. (14). In later analysis, we will see that these decaying terms will be initiated whenever the signal moves to a new segment.

3.2 System Model When $\varepsilon \neq 0$ and Coordinates Transform. For more accurate approximation, we consider $\varepsilon \neq 0$ in this subsection. The system (9) is written in the general form

$$\begin{bmatrix}\dot{x}\\ \varepsilon\dot{z}\end{bmatrix} = \begin{bmatrix}A_{11} & A_{12}\\ A_{21} & A_{22}\end{bmatrix}\begin{bmatrix}x\\ z\end{bmatrix} + \begin{bmatrix}B_1\\ B_2\end{bmatrix}y_r + \begin{bmatrix}0\\ \gamma'\end{bmatrix} \tag{15}$$

where $A_{11} = 0$, $A_{12} = -C$, $B_1 = 1$ and (A_{21}, A_{22}, B_2, and γ') are the corresponding matrix/vector coefficients of x, z, y_r and the constant term of Eq. (9), respectively. We keep $O(\varepsilon)$ terms of

the series expansion and sum the rest as $O(\varepsilon^2)$. We use the following transformation [31], which allows us to separate the slow and fast variables:

$$\begin{bmatrix} \xi \\ \eta \end{bmatrix} = \begin{bmatrix} (I_n - \varepsilon \mathscr{H}\mathscr{L}) & -\varepsilon\mathscr{H} \\ \mathscr{L} & I_m \end{bmatrix} \begin{bmatrix} x \\ z \end{bmatrix} + \begin{bmatrix} \varepsilon\mathscr{H}W \\ -W \end{bmatrix} y_r \tag{16}$$

where ξ is the slow variable and η is the fast variable in the new coordinates. I_n and I_m are identity matrices of the dimensions of the slow and fast variables, respectively. W is a constant vector of the dimension of the fast variable. $\mathscr{L}$ and $\mathscr{H}$ are analytical functions of ε. To get back to the original coordinates, we use the inverse of the above transformation:

$$\begin{bmatrix} x \\ z \end{bmatrix} = \begin{bmatrix} I_n & \varepsilon\mathscr{H} \\ -\mathscr{L} & (I_m - \varepsilon\mathscr{L}\mathscr{H}) \end{bmatrix} \begin{bmatrix} \xi \\ \eta \end{bmatrix} + \begin{bmatrix} 0 \\ W \end{bmatrix} y_r \tag{17}$$

Since we are interested in an $O(\varepsilon^2)$ approximation, we use the approximations $\mathscr{L} = L + \varepsilon A_{22}^{-2} A_{21} A_0 + O(\varepsilon^2)$ and $\mathscr{H} = H + \varepsilon A_1 + O(\varepsilon^2)$, where $L = A_{22}^{-2} A_{21}, H = A_{12} A_{22}^{-1}$, $A_1 = (A_0 H - H L A_{12}) A_{22}^{-1}$, and $A_0 = A_{11} - A_{12} A_{22}^{-1} A_{21}$ is a scalar. We follow similar steps as in Ref. [31] to derive the system model in the new coordinates. We note that in Ref. [31] the driving term does not exist. This term will allow us to discuss the dependence of the solution on the reference frequency ω. By ignoring the $O(\varepsilon^2)$ terms in all coefficients, we arrive at the following equations in which the slow and fast models are separated:

$$\begin{aligned} \dot{\xi} = {} & (A_0 - \varepsilon H L A_0)\xi + [-\varepsilon H L A_{12} W - H B_2 - \varepsilon A_1 B_2 \\ & + (I_n - \varepsilon H L) B_1] y_r + \varepsilon H W \dot{y}_r - H\gamma' - \varepsilon A_1 \gamma' \end{aligned} \tag{18}$$

$$\begin{aligned} \varepsilon\dot{\eta} = {} & (A_{22} + \varepsilon L A_{12})\eta + (B_2 + \varepsilon L B_1 + (A_{22} + \varepsilon L A_{12}) W) y_r \\ & + \gamma' - \varepsilon W \dot{y}_r \end{aligned} \tag{19}$$

We solve Eqs. (18) and (19) to get the expression of the tracking error e as follows. First for ξ, we express the solution of Eq. (18) as a power series

$$\xi = \xi_0 + \varepsilon\xi_1 + \varepsilon^2\xi_2 + \ldots \tag{20}$$

By matching ε-coefficients of Eq. (18) and the derivative of ξ of Eq. (20), we obtain

$$\dot{\xi}_0 = A_0\xi_0 + B_0 y_r - H\gamma' \tag{21}$$

$$\begin{aligned} \dot{\xi}_1 = {} & A_0\xi_1 - H L A_0 \xi_0 + [-H L A_{12} W - B_1 H L - A_1 B_2] y_r \\ & + H W \dot{y}_r - A_1 \gamma' \end{aligned} \tag{22}$$

where $B_0 = [-HB_2 + B_1]$. In order to see how the solution develops and the error propagates from one hysteresis segment to another, we solve the equations for each segment by dividing the time into intervals that correspond to the time periods of the hysteresis staying in different segments. We specify the time at the beginning of each slot by t_i, where $i = 0, 1, \ldots$. Then, for the current segment i, we have the time t bounded as $t_i \leqq t < t_{i+1}$. See Fig. 4 for illustration.

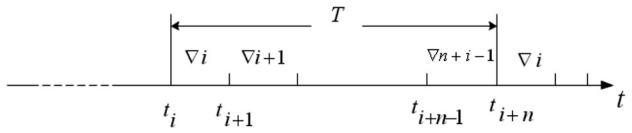

Fig. 4 Illustration of the time instants when periodic signals cross different linear segments of the hysteresis loops

3.3 The Case of a Sinusoidal Reference. We now consider a sinusoidal reference $y_r = A_c \sin(\omega t)$. We assume that the solution of the closed-loop system converges to a periodic function with the same period T of the reference input. This assumption is justified by the simulation and experimental results in this work and also in Refs. [11,14,16,17,23]. Moreover, we assume that all the components which compose the solution such as the slow ξ and fast η variables are periodic.

The idea of getting a solution that shows the impact of all hysteresis segments on each other is explained by the following steps. We start by solving Eq. (21) for the segment i with initial value $\xi_0(t_i)$. Then, the final value of this segment $\xi_0(t_{i+1})$ will be inserted as the initial value for the following segment $i+1$. We continue this process around one cycle until we get $\xi_0(t_i + T)$. The periodicity of the solution implies that $\xi_0(t_i + T) = \xi_0(t_i)$ and this allows us to obtain an expression for $\xi_0(t_i)$. By substituting this expression in the solution of Eq. (21) we get $\xi_0(t), t_i \leq t < t_{i+1}$

$$\xi_0(t) = \varphi + \frac{H\gamma'}{A_0} + B_0 A_c \left(\frac{A_0}{A_0^2 + \omega^2} \sin(\omega t) \frac{\omega}{A_0^2 + \omega^2} \cos(\omega t) \right) \tag{23}$$

where φ is in the form

$$\varphi = e^{A_{0i}(t - t_i)} \sum_{j=1}^{n} e^{-A_{0j} K_j} \left(\frac{L_j}{A_{0j}} + \frac{M_j \omega}{A_{0j}^2 + \omega^2} + \frac{N_j A_{0j}}{A_{0j}^2 + \omega^2} \right) \tag{24}$$

n is the number of hysteresis segments traversed in one cycle, and K_j, L_j, M_j, and N_j are constants dependent on the parameters of the j-th segment in the cycle. The complete derivation of $\xi_0(t)$ is given in Appendix A. The complete derivation of the bound on φ can be found in Ref. [32]. The term φ can be described by a periodic term, which has a peak value at the beginning of each segment and decays exponentially with a rate dependent on the value A_0 until the following segment. φ is important in the sense that it connects the solutions of different segments by summing the propagated error of all previous segments in each cycle. However, this term can be made small by a choice of a large value of $|A_0|$. Since the choice of A_0 is important, let us derive its expression and see how it changes from one segment to another

$$\begin{aligned} A_0 &= A_{11} - A_{12} A_{22}^{-1} A_{21} \\ &= 0 - C \left[A - k_p \frac{m + \Delta_m}{m} BC \right]^{-1} B \frac{m + \Delta_m}{m} k_i \\ &= \frac{-(m + \Delta_m) k_i h}{1 + k_p (m + \Delta_m) h} \end{aligned} \tag{25}$$

With the assumption that the slopes of all segments are positive $(m > 0)$, we also need to assume $|\Delta_m| < m$, or equivalantly $m + \Delta_m > 0$, for all segments, such that $A_0 < 0$. By choosing k_p such that $k_p(m + \Delta_m)h$ is much larger than 1, A_0 becomes independent of the segment slope and is determined by the ratio k_i/k_p. By having the integral gain much larger than the proportional gain $(k_i \gg k_p)$, we guarantee that $|A_0|$ is large enough to make the value of φ significantly small and decays in a short time within each segment.

In Appendix B, we show that ξ_1 is bounded uniformly in ω. Hence, the slow variable ξ is obtained by substituting ξ_0 from Eq. (23) into Eq. (20). The solution of the fast variable is derived in Appendix C as

$$\begin{aligned} \eta = {} & \psi - A_\eta^{-1} B_\eta A_c \sin(\omega t) - A_\eta^{-1} \gamma' \\ & + \varepsilon (A_\eta^{-1} W - A_\eta^{-2} B_\eta) A_c \omega \cos(\omega t) + O(\varepsilon^2) \end{aligned} \tag{26}$$

where $A_\eta = (A_{22} + \varepsilon L A_{12}), B_\eta = B_2 + \varepsilon L B_1 + (A_{22} + \varepsilon L A_{12})W)$, and ψ is a term similar to the φ term of the slow variable, but it decays much faster than φ. The tracking error for $t_i \le t < t_{i+1}$ in terms of ξ and η is given by

$$\begin{aligned} e(t) &= B_1 y_r - Cz \\ &= B_1 y_r - A_{12}\left[(L + \varepsilon A_{22}^{-2} A_{21} A_0)\xi \right. \\ &\quad \left. + (I_m - \varepsilon L H)\eta + W y_r\right] + O(\varepsilon^2) \\ &= -A_{12}(L + \varepsilon A_{22}^{-2} A_{21} A_0)\xi + A_{12}\eta - \varepsilon A_{12} L H \eta \\ &\quad + (B_1 + A_{12}W) y_r + O(\varepsilon^2) \end{aligned} \tag{27}$$

By inserting ξ from Eqs. (23) and (20) and η from Eq. (26) into Eq. (27) we obtain the final expression of the error with its $O(\varepsilon^2)$ approximation

$$\begin{aligned} e(t) &= (B_1 + A_{12}W) y_r + A_{0i}\left[\varphi + \frac{H_i \gamma_i'}{A_{0i}} \right. \\ &\quad + B_{0i} A_c \left(\frac{A_{0i}}{A_{0i}^2 + \omega^2}\sin(\omega t) - \frac{\omega}{A_{0i}^2 + \omega^2}\cos(\omega t)\right) \\ &\quad \left. + \varepsilon \xi_1\right] - \varepsilon A_{12} A_{22}^{-2} A_{21} A_{0i} \xi_0 + A_{12}\left[-A_{\eta,i}^{-1} B_{\eta,i} A_c \sin(\omega t)\right. \\ &\quad \left. + \psi - A_{\eta,i}^{-1}\gamma' + \varepsilon(A_{\eta,i}^{-1} W - A_{\eta,i}^{-2} B_{\eta,i}) A_c \omega \cos(\omega t)\right] \\ &\quad - \varepsilon A_{12} L H[-A_{\eta,i}^{-1} B_{\eta,i} A_c \sin(\omega t) - A_{\eta,i}^{-1}\gamma'] + O(\varepsilon^2) \end{aligned} \tag{28}$$

To discuss how these terms change with the frequency, we separate the error expression into three groups

$$e = e_0 + \varepsilon e_\varepsilon + \varepsilon\omega e_{\varepsilon\omega} + O(\varepsilon^2) \tag{29}$$

where e_0, e_ε, and $e_{\varepsilon\omega}$ are bounded uniformly in ε and ω. In other words, $|e_0| \le k_1, |e_\varepsilon| \le k_2$, and $|e_{\varepsilon\omega}| \le k_3$, where k_1, k_2, and k_3 are some positive constants independent of ϵ and ω. The contribution from the e_ε term can be ignored because it is multiplied by a small number ε. The term $e_{\varepsilon\omega}$ becomes significant at high frequencies when its coefficient $\varepsilon\omega$ is not small. Let us start with analyzing the e_0 term. By ignoring $O(\varepsilon)$ terms, A_η^{-1} can be approximated by A_{22}^{-1} and the term $-A_{12}A_\eta^{-1}$ is replaced by $-H$. Then $H\gamma'$ cancels out the term $-A_{12}A_\eta^{-1}\gamma'$, resulting in

$$\begin{aligned} e_0(t) &= (B_1 + A_{12}W) y_r + A_0\left[\varphi + B_0 A_c\left(\frac{-A_0}{A_0^2 + \omega^2}\sin(\omega t)\right.\right. \\ &\quad \left.\left. - \frac{\omega}{A_0^2 + \omega^2}\cos(\omega t)\right)\right] - A_{12}A_\eta^{-1} B_\eta A_c \sin(\omega t) + A_{12}\psi \end{aligned} \tag{30}$$

$B_1 = 1$ and W can be chosen such that $A_{12}W = -1$ and the first term is eliminated. This is always possible because $A_{12} = -C$ is rank 1 and it is a row vector with all of its elements zeros except the element representing the output of the linear plant. We can also show that $-A_{12}A_\eta^{-1}B_\eta = 1 - HB_2 = B_0$ and simplify the equation by combining sine terms together, which produces $B_0 A_c(\omega^2/(A_0^2 + \omega^2))\sin(\omega t)$. B_η is approximated by $B_2 + A_{22}W$ and multiplied by $-A_{12}A_{22}^{-1}$ to get $1 - H B_2$ and then replaced in Eq. (30). Then, $e_0(t)$ becomes

$$e_0(t) = A_0\varphi + B_0\frac{\omega^2}{A_0^2 + \omega^2} A_c \sin(\omega t) + A_{12}\psi \tag{31}$$

It is noted that for a sufficiently high frequency ($|A_0| \ll \omega \ll 1/\varepsilon$), $(\omega^2/A_0^2 + \omega^2)$ becomes constant and almost independent on frequency. The $\varepsilon\omega e_{\varepsilon\omega}$ term is

$$\varepsilon\omega e_{\varepsilon\omega}(t) = A_{12}[A_\eta^{-1}\varepsilon W - \varepsilon A_\eta^{-2} B_\eta]\omega A_c \cos(\omega t) \tag{32}$$

By replacing $A_{12}[A_\eta^{-1}]$ by H in Eq. (32), we have

$$\begin{aligned} \varepsilon\omega e_{\varepsilon\omega}(t) &= \varepsilon(HW - H A_\eta^{-1} B_\eta)\omega A_c \cos(\omega t) \\ &= \varepsilon(HW - H A_{22}^{-1}(B_2 + A_{22}W))\omega A_c \cos(\omega t) \\ &= -\varepsilon(H A_{22}^{-1} B_2)\omega A_c \cos(\omega t) \end{aligned} \tag{33}$$

By ignoring $\varepsilon e_\varepsilon$ and $O(\varepsilon^2)$ in Eq. (29) and substituting e_0 from Eq. (31) and $\varepsilon\omega e_{\varepsilon\omega}$ from Eq. (33) into Eq. (29), we obtain an approximate expression for the error during each segment i for a sufficiently high frequency ($|A_0| \ll \omega \ll 1/\varepsilon$)

$$\begin{aligned} e(t) &= A_0\varphi + B_0 A_c \frac{\omega^2}{A_0^2 + \omega^2}\sin(\omega t) \\ &\quad - \varepsilon(H A_{22}^{-1} B_2)\omega A_c \cos(\omega t) + A_{12}\psi \end{aligned} \tag{34}$$

In summary, the bound on the tracking error is composed of two components. The decaying component, which is represented by $A_0\varphi + A_{12}\psi$, has its peak at the beginning of each segment and its contribution can be reduced by the choice of control gains. The nondecaying component has the following characteristics. At a very low frequency ($\omega \ll |A_0|$), the error is proportional to the frequency. This is due to the sine term of Eq. (34). Then, by increasing the frequency, we reach a range where the error becomes almost constant with a value that depends on the system parameters and uncertainties, $B_0 A_c$ of Eq. (34). Then, it starts to increase linearly with the frequency again when $\varepsilon\omega$ of the third term of Eq. (34) becomes large enough to contribute to the total amount of the error. This is true as long as the $O(\varepsilon^2)$ approximation is valid.

3.4 Bound on All Segments. The error expression (34) is valid for each segment. Let us again use the subscript i to denote each segment. By taking the absolute value of e and using the triangular inequality, we obtain

$$|e_i| \le |A_{0i}\varphi_i| + |B_{0i}A_c| + |\varepsilon(H_i A_{22,i}^{-1} B_{2,i})|\omega A_c + |A_{12}\psi_i| \tag{35}$$

The upper bound $|e|_{\max}$ of the error for all segments can be determined by studying when the highest value of each term in Eq. (35) occurs. Let us start with the second term $|B_{0i}|$. Note

$$B_{0i} = 1 - H_i B_2 = 1 - A_{12}A_{22}^{-1}B_2 \tag{36}$$

Then substituting the matrices A_{12}, A_{22}^{-1}, and B_2 from Eq. (9) into Eq. (36), we get

$$B_{0i} = 1 - C\left[A - k_p\frac{m_i + \Delta_{m_i}}{m_i}BC\right]^{-1} B\frac{m_i + \Delta_{m_i}}{m_i}(g + k_p) \tag{37}$$

Using the matrix inversion lemma, we simplify $C[A - k_p((m_i + \Delta_{m_i})/m_i)BC]^{-1}B$ to

$$C\left[A - k_p\frac{m_i + \Delta_{m_i}}{m_i}BC\right]^{-1} B = \frac{-m_i h}{m_i + k_p(m_i + \Delta_{m_i})h} \tag{38}$$

Then, we insert Eq. (38) into Eq. (37) to get

$$B_{0i} = \frac{m_i(1 - gh) - \Delta_{m_i} gh}{m_i + k_p(m_i + \Delta_{m_i})h} \tag{39}$$

This expression appears as the coefficient of the driving term of Eq. (11). By taking the feedforward gain $g = 1/h$, we get

$$B_{0i} = \frac{-\Delta_{m_i}}{m_i + k_p(m_i + \Delta_{m_i})h} \tag{40}$$

Let us denote the bound on B_{0i} By $B_{0,\max}$ for all segments. This is obtained by substituting the largest $|\Delta_m|_{\max}$ in the numerator and the smallest $m_{\min}$ in the denominator of Eq. (39)

$$|B_0|_{\max} < \frac{|\Delta_m|_{\max}}{m_{\min} + k_p(m_{\min})h} \tag{41}$$

The bound $|\psi|_{\max}$ on all segments is derived in Appendix C. The upper bound $(HA_{22}^{-1}B_2)_{\max}$ on the third term of Eq. (35) is given in Appendix D. We find that this high-frequency term is nearly independent of m and Δ_m for the case $|\Delta_m| < m$. In other words, this term does not change much from one segment to another. More details of derivations can be found in Ref. [32].

We conclude that the upper bound of the error can be determined by substituting m_i by $m_{\max}$ and Δ_{m_i} by $|\Delta_m|_{\max}$ in the numerator and m_i by $m_{\min}$ in the denominator. Applying this to $|A_{0i}|$ we obtain $|A_0|_{\max}$ which replaces A_{0i} for the upper-bound on the error

$$|e|_{\max} \le |A_0|_{\max}|\varphi|_{\max} + |B_0|_{\max}A_c + |-\varepsilon(HA_{22}^{-1}B_2)_{\max}|\omega A_c + |A_{12}\psi|_{\max} \tag{42}$$

3.5 The Case of Periodic References. The earlier analysis for the case of a sinusoidal reference can be extended to the case of a general periodic reference. We have found from the solutions of the slow and fast variables in the case of a sinusoidal reference that the steady-state solution contains two parts. One has a decaying form and is dependent on all previous segments of the hysteresis loop. The other is only dependent on the current segment and is obtained by solving an integral equation as in the conventional linear system. It is easy to show that a similar procedure can be applied to any periodic reference. For instance

$$\xi_0(t) = \phi_i + \frac{H_i\gamma_i'}{A_{0i}} + \int_{t_i}^{t} e^{A_{0i}(t-\tau)}B_{0i}y_r(\tau)d\tau \tag{43}$$

where ϕ_i is given by

$$\begin{aligned}\phi_i = \frac{e^{A_{0i}(t-t_i)}}{1-M}\Bigg[& e^{A_{0,i+n-1}\Delta_{i+n-1}}\cdots e^{A_{0,i+1}\Delta_{i+1}}\left(\left(\frac{H_i\gamma_i'}{A_{0i}} - \frac{H_{i+1}\gamma_{i+1}'}{A_{0,i+1}}\right) + e^{A_{0i}t_{i+1}}\int_{t_i}^{t_{i+1}} e^{-A_{0i}\tau}B_{0i}y_r(\tau)d\tau\right) \\ & + \cdots \\ & + e^{A_{0,i+n-1}\Delta_{i+n-1}}\left(\left(\frac{H_{i+n-2}\gamma_{i+n-2}'}{A_{0,i+n-2}} - \frac{H_{i+n-1}\gamma_{i+n-1}'}{A_{0,i+n-1}}\right) + e^{A_{0,i+n-2}t_{i+n-1}}\int_{t_{i+n-2}}^{t_{i+n-1}} e^{-A_{0,i+n-2}\tau}B_{0,i+n-2}y_r(\tau)d\tau\right) \\ & + \left(\left(\frac{H_{i+n-1}\gamma_{i+n-1}'}{A_{0,i+n-1}} - \frac{H_i\gamma_i'}{A_{0i}}\right) + e^{A_{0,i+n-1}t_{i+n}}\int_{t_{i+n-1}}^{t_{i+n}} e^{-A_{0,i+n-1}\tau}B_{0,i+n-1}y_r d\tau\right)\Bigg]\end{aligned} \tag{44}$$

and M is defined as

$$M = e^{A_{0,i+n-1}\Delta_{i+n-1}}\cdots e^{A_{0,i+1}\Delta_{i+1}}e^{A_{0,i}\Delta_i} \tag{45}$$

and $\Delta_i = t_{i+1} - t_i$. The fast variable η is derived for any periodic reference in Eq. (C5) in Appendix C. Then, for a given periodic input $y_r(t)$ we solve the integration of Eq. (43) and substitute ξ and η in Eq. (27) to obtain the expression of the tracking error.

Since any periodic signal is bounded by a constant K, $|y_r| \le K$, an upper bound on ϕ_i can be obtained by replacing y_r by K in Eq. (44) to get

$$\begin{aligned}|\phi_i| \le \frac{e^{A_{0i}(t-t_i)}}{1-M}\Bigg[& M\left|\frac{B_{0,i}K}{A_{0,i}}\right| + e^{A_{0,i+n-1}\Delta_{i+n-1}}\cdots e^{A_{0,i+1}\Delta_{i+1}}\left(\left|\frac{H_i\gamma_i'}{A_{0i}} - \frac{H_{i+1}\gamma_{i+1}'}{A_{0,i+1}}\right| + \left|\frac{B_{0i}K}{A_{0i}}\right| + \left|\frac{B_{0,i+1}K}{A_{0,i+1}}\right|\right) \\ & + \cdots \\ & + e^{A_{0,i+n-1}\Delta_{i+n-1}}\left(\left|\frac{H_{i+n-2}\gamma_{i+n-2}'}{A_{0,i+n-2}} - \frac{H_{i+n-1}\gamma_{i+n-1}'}{A_{0,i+n-1}}\right| + \left|\frac{B_{0,i+n-2}K}{A_{0,i+n-2}}\right| + \left|\frac{B_{0,i+n-1}K}{A_{0,i+n-1}}\right|\right) \\ & + \left|\frac{H_{i+n-1}\gamma_{i+n-1}'}{A_{0,i+n-1}} - \frac{H_i\gamma_i'}{A_{0i}}\right| + \left|\frac{B_{0,i+n-1}K}{A_{0,i+n-1}}\right|\Bigg]\end{aligned} \tag{46}$$

Although the bound on $|\phi_i|$ looks different from the one obtained in the case of a sinusoidal reference, they both can be made small by increasing the value of $|A_{0i}|$. However, in the case of a sinusoidal reference we have the full solution with the coefficients $A_{0i}/(A_{0i}^2 + \omega^2)$ or $\omega/(A_{0i}^2 + \omega^2)$ appearing instead of $1/A_{0i}$, which shows that this bound is smaller in high frequencies, $\omega > |A_{0i}|$. We should note that increasing the value of $|A_0|$ reduces the value of $|\varphi|$, but this does not help much with the tracking error because we multiply φ by A_0 when the error is calculated.

4 Simulation and Experimental Results

The simulation is based on the model and parameters identified experimentally for a commercial nanopositioner. Details of the experiments are provided in Sec. 4.2. The linear dynamics are fitted experimentally with a second-order system with a natural frequency of 2086 Hz, which corresponds to $\varepsilon = 7.63 \times 10^{-5}$. The hysteresis is modeled with a PI operator with 5 play operators with thresholds $r = [0,\ 0.63,\ 1.27,\ 2.54,\ 4.45]^T$ and the vector of weights for the operator is $w^T = [5.88,\ 1.58,\ 0.47,\ 0.98,\ 0.4]$. When we apply a periodic reference signal (with single maximum and minimum in each period) with amplitude 50 μm, we obtain a loop of five segments in the ascending side and similarly in the descending side at steady state. The slopes of the ascending side of the loop are $(m_1 = 0.67,\ m_2 = 0.85,\ m_3 = 0.9,\ m_4 = 1.01,\ m_5 = 1.057)$. The slopes of the descending side of the loop are $(m_6 = 0.67,\ m_7 = 0.85,\ m_8 = 0.9,\ m_9 = 1.01,\ m_{10} = 1.057)$. The intercepts are $(\gamma_1 = -6.8, \gamma_2 = -3.31, \gamma_3 = -2.58, \gamma_4 = -2.8, \gamma_5 = -2.9, \gamma_6 = 6.8, \gamma_7 = 3.31, \gamma_8 = 2.58,\ \ \gamma_9 = 2.8, \gamma_{10} = 2.9)$. The weight vector of the operator is perturbed for the simulation purpose by adding 0.15 for each element of w. This perturbation changes the slopes of the loop and is equivalent to uncertainties as $(\Delta_{m1} = 0.016, \Delta_{m2} = 0.03, \Delta_{m3} = 0.05,\ \Delta_{m4} = 0.07,\ \Delta_{m5} = 0.08, \Delta_{m6} = 0.016, \Delta_{m7} = 0.03,\ \Delta_{m8} = 0.05, \Delta_{m9} = 0.07, \Delta_{m10} = 0.08)$ and $(\Delta_{\gamma 1} = -1.0313,\ \Delta_{\gamma 2} = -0.7,\ \Delta_{\gamma 3} = -0.46,\ \Delta_{\gamma 4} = -0.413, \Delta_{\gamma 5} = -0.7,\ \Delta_{\gamma 6} = 1.0313,\ \Delta_{\gamma 7} = 0.7,\ \Delta_{\gamma 8} = 0.46,\ \Delta_{\gamma 9} = 0.413, \Delta_{\gamma 10} = 0.7)$. Note that all simulation and experimental results are presented for the case when the feedforward component is added if we do not mention otherwise. We only present the case without feedforward only when we want to compare the two cases.

4.1 Simulation Results Versus Analytical Results. Figures 5 and 6 show the simulation for a reference consisting of two sinusoids and a sawtooth reference signal, respectively, where the hysteresis uncertainty is included. The uncertainties are introduced by perturbing the weights of play operators, as explained earlier. We observe that, in each case, the tracking error is also periodic with the same period as the reference. We also observe that the tracking error has a similar waveform as the reference input but it is distorted when the slope changes from one segment to another.

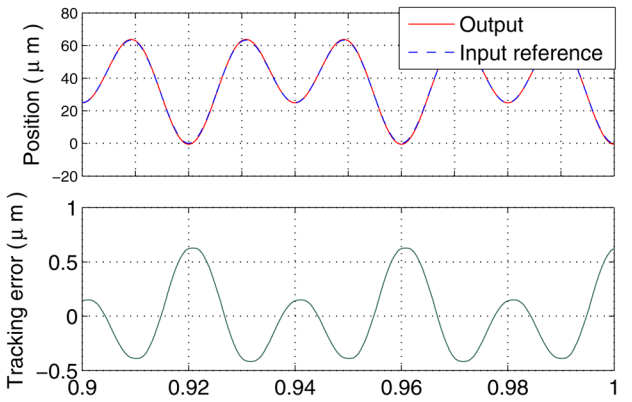

Fig. 5 Simulations results on tracking a periodic reference composed of two sinusoidal signals of 25 Hz and 50 Hz

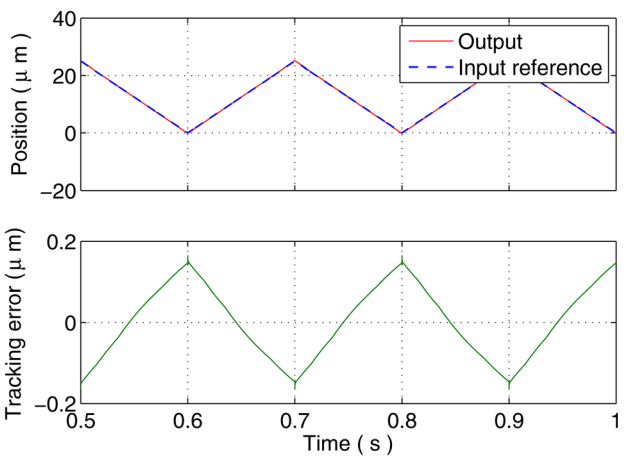

Fig. 6 Simulation results on tracking a sawtooth reference of 5 Hz

The change in slopes is more obvious in the case of the triangular waveform. Figure 7 depicts the tracking errors for the same triangular input reference of 5 Hz with and without feedforward term, where perfect hysteresis inversion is assumed. From these results we confirm that feedforward-augmented feedback outperforms feedback alone. Further simulation results involving the sawtooth reference are depicted in Fig. 8, where we compare the tracking errors when uncertainty are present and absent in the hysteresis model, respectively. From Fig. 8, the influence of the model uncertainty on the tracking error is evident. The size of the error for each segment is dependent on the segment slope and may be large or small depending on the value of m at that segment.

In Table 1, we compare the maximum amplitudes of the tracking error, when the reference signal is a sinusoid with amplitude of 50 μm and its range of frequencies is 1–1000 Hz. Here, we adopt the control scheme with the feedforward term and consider the model uncertainty as discussed earlier. The gains for the proportional-integral controller are chosen as $k_i = 50$ and $k_p = 3$. Moreover, a comparison between simulation and analytical results is provided. These results are also plotted in Fig. 9 for a better illustration. The identified second-order plant is used in the calculation of the analytic results. The value of φ is provided in Table 1, which shows that it has little effect on calculating the error especially at high frequencies. The maximum contribution of ψ to the error, which is calculated but not included in Table 1, is $|A_{12}\psi|_{\max} = 0.0948$. This term is almost constant when the frequency is increased. From Table 1 and Fig. 9, we notice the following. First, for this particular example, the ϕ term is small and can be ignored for all frequencies of 10 Hz or higher. Second, the

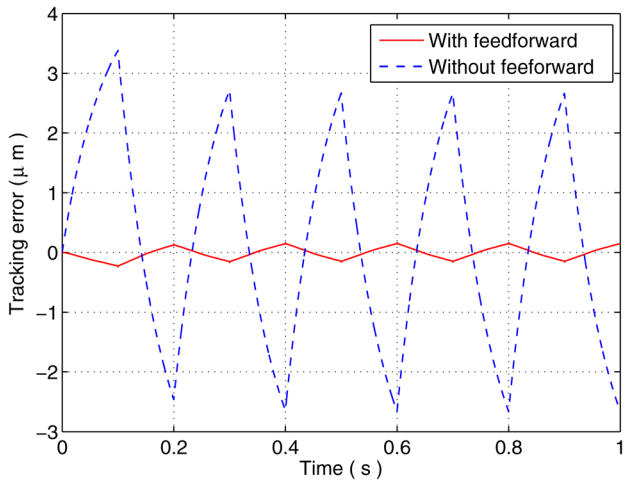

Fig. 7 Simulation results on tracking a sawtooth reference with and without feedforward compensation

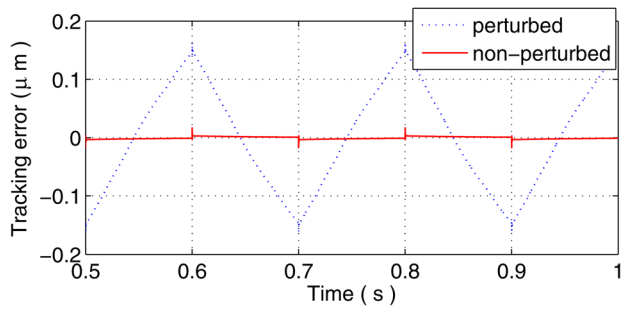

Fig. 8 Simulation results on tracking a sawtooth reference when uncertainty is present/absent in the hysteresis model

Table 1 Simulation and analytical results on maximum tracking errors in μm for a system involving a perturbed PI-operator and a second-order plant

Frequency	Simulation Max $\lvert e(t)\rvert$	Analytical Max $\lvert e(t)\rvert$	φ Max $\lvert\varphi\rvert$
1 Hz	0.177	0.26	0.019
10 Hz	0.375	0.57	0.009
20 Hz	0.38	0.58	0.004
50 Hz	0.39	0.586	0.001
80 Hz	0.41	0.592	3×10^{-4}
100 Hz	0.42	0.597	5×10^{-5}
150 Hz	0.475	0.61	2.6×10^{-4}
200 Hz	0.53	0.63	4.2×10^{-4}
400 Hz	0.82	0.77	6.9×10^{-4}
600 Hz	1.2	0.95	7.3×10^{-4}
800 Hz	1.66	1.16	7.7×10^{-4}
1000 Hz	2.2	1.38	7.9×10^{-4}

error obtained in simulation increases with the frequency at low frequencies, then it remains almost constant for the mid-frequency range, and then it starts to increase again with frequency. This is consistent with the error bound we calculated in Sec. 3.4. Third, the calculated error bound is close to the error from the simulation. This bound is good up to 200 Hz, because we use $O(\varepsilon^2)$ approximation which is valid for $\omega \ll 1/\varepsilon$. It is clear from these results that when frequencies become closer to the closed-loop system bandwidth, we should consider approximations better than $O(\varepsilon^2)$ approximation.

In Fig. 10, we further study the effect of PI controller gains, k_i and k_p, on the tracking performance, where three new sets of PI

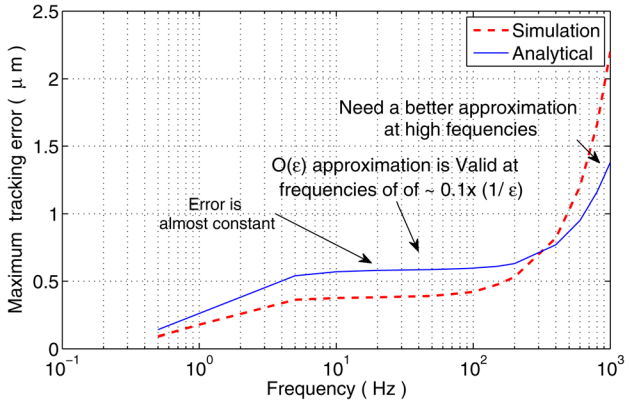

Fig. 9 Comparison of simulation and analytical results on the tracking error as the reference frequency is varied

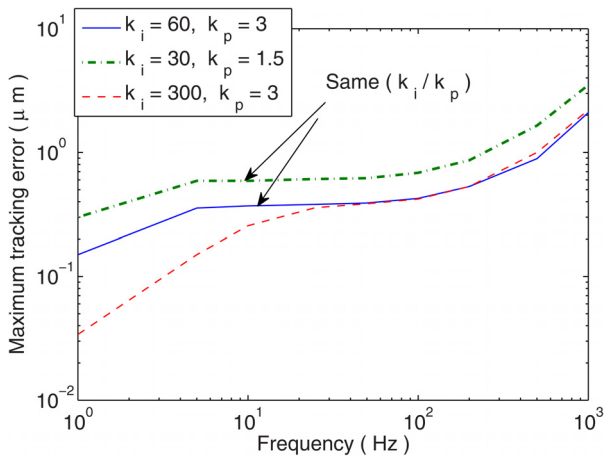

Fig. 10 Comparison of the amplitude of tracking error for different control gains as the reference frequency is varied

gains are used in simulations. From our analysis we found that $A_0 \simeq (k_i/k_p)$ determines the shape of the tracking-error frequency response. As shown in the figure, two plots with $k_i/k_p = 20$ have similar frequency responses, with only a shift between them where the plot with higher k_i and k_p has smaller error. We also note that by increasing k_i only, a reduction occurs in the error in the low-frequency range. At high frequencies, we could reduce the error by increasing the gain k_p; however, that is constrained by closed-loop stability.

4.2 Experimental Results. A commercial piezo-actuated nanopositioner (Nano-OP65 with Nano Drive controller, Mad City Labs Inc.,) is used in the experiments. Displacement feedback for the positioner is provided by a built-in capacitive sensor. A dSPACE system (DS1104, dSPACE Inc.,) is adopted to interface between the voltage input/displacement output of the nanopositioner with a PC. The nanopositioner is mounted on a vibration-isolation table (LW3048B-OPT, Newport) to minimize the impact of ambient vibrations. In the experiments, an important safety mechanism implemented is a rate limiter, to protect the nanopositioner from sudden changes of the applied voltage input.

In experiments, sinusoidal signals are first used as reference trajectories in order to examine how the tracking error depends on the frequency. Figure 11 shows the tracking performance for a 35 Hz sinusoidal reference with amplitude of 20 μm when the feedforward is used. Figure 12 compares the tracking errors for references of different frequencies, 10 Hz, 35 Hz, and 50 Hz. For the best results, the control gains are chosen as $k_i = 2000$ and

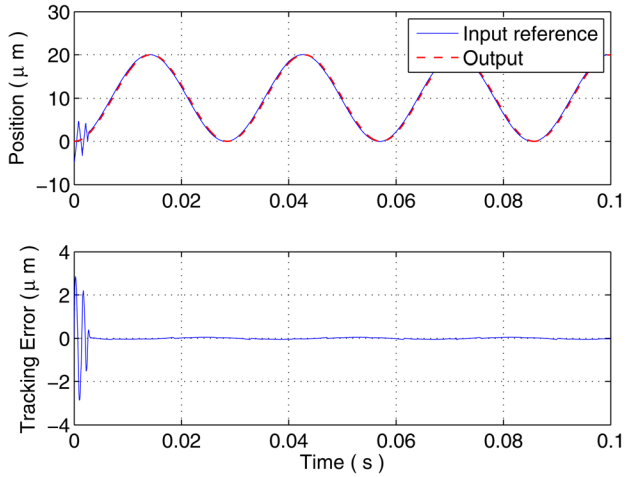

Fig. 11 Experimental results on the tracking performance of a 35 Hz sinusoidal reference

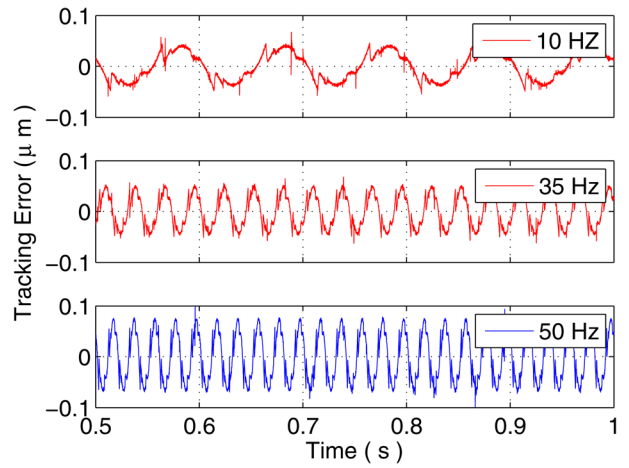

Fig. 12 Experimental results on the tracking error for sinusoidal references of different frequencies

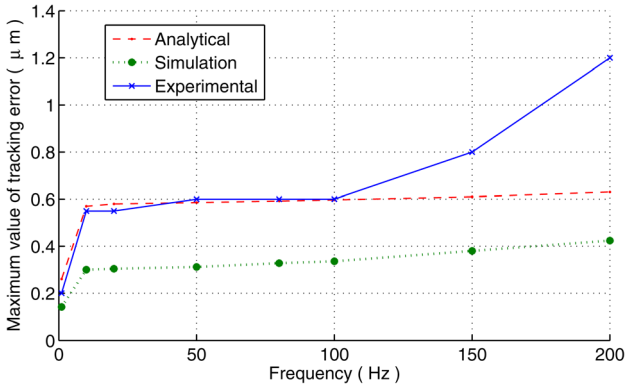

Fig. 13 Comparison of simulation, analytical, and experimental results on the tracking error as the reference frequency is varied

$k_p = 1.5$. The maximum tracking error is about 0.05 μm and slightly increases through the range from 10 Hz to 35 Hz. We see a larger increase of about 0.08 μm at 50 Hz. We also compare the experimental results with analysis and simulations for the range of frequencies from 1 to 200 Hz. The results in Fig. 13 show a similar qualitative behavior of the tracking error for the analytical,

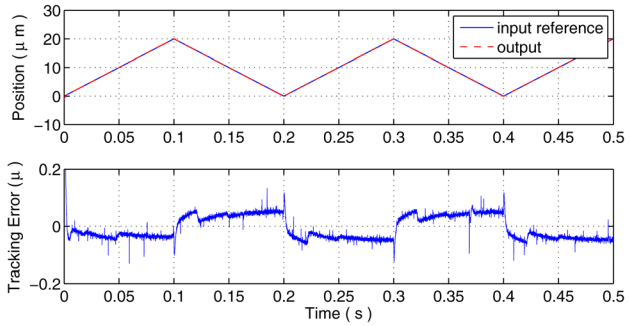

Fig. 14 Experimental results on the tracking of a triangular reference

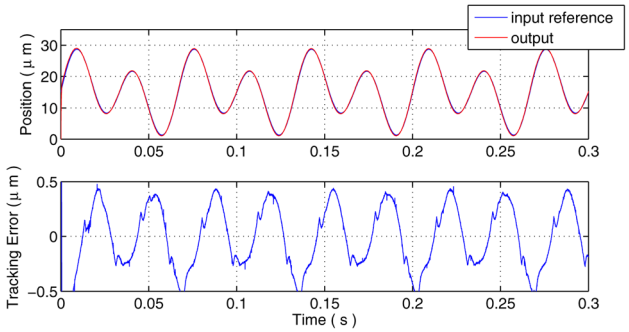

Fig. 15 Experimental results on the tracking of a multisine reference with frequencies of 15 Hz and 30 Hz

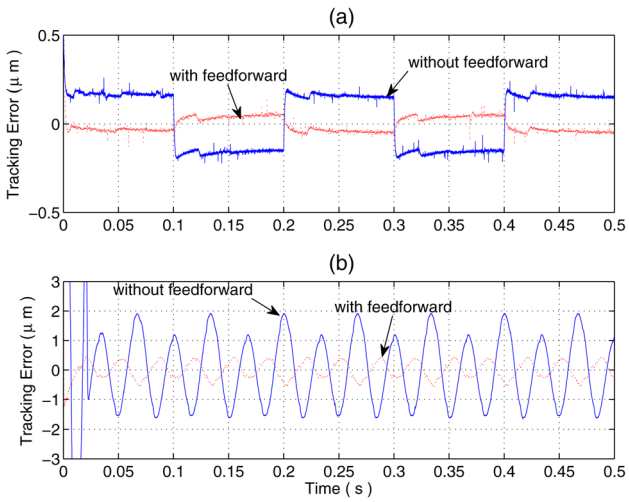

Fig. 16 Comparison of tracking errors with and without the feedforward component for (*a*) a triangular reference and (*b*) mutisine reference

simulation, and experimental results. It is found that the experimental error is very close to the analytical bound at relatively low frequencies (lower than 100 Hz). But at higher frequencies, the experimental error is larger than and deviates from the bound. This is attributed to the impact of the rate limiter implemented in experiments but not included in the analysis; in particular, the rate limiter modifies the control input to meet the rate constraint, which distorts the original control signal when tracking relatively high-frequency references.

Experiments have also been conducted to examine the performance of tracking triangular and multisine reference signals, the results of which are shown in Figs. 14 and 15, respectively, where

Table 2 Experimental results on maximum tracking errors in μm with and without feedforward compensation

Frequency	With feedforward Max $\lvert e(t)\rvert$	Without feedforward Max $\lvert e(t)\rvert$
1 Hz	0.02	0.025
10 Hz	0.04	0.2
20 Hz	0.045	0.38
50 Hz	0.08	0.8
80 Hz	0.11	1.4
100 Hz	0.12	1.7
150 Hz	0.32	2.2
200 Hz	0.6	3.0

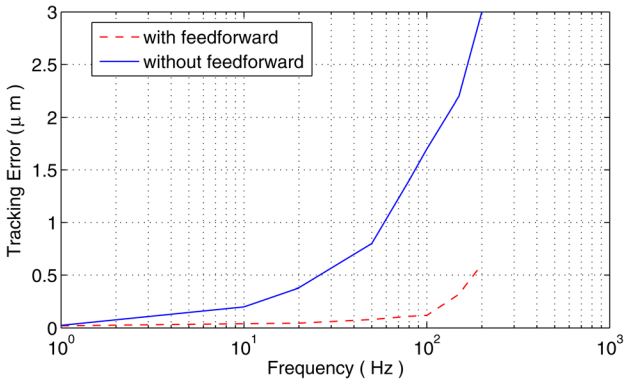

Fig. 17 Comparison of tracking error with and without feedforward component for a sinusoidal reference

the PI control with feedforward is used. Figure 16 shows a comparison of the tracking errors when the feedforward is present or absent for the triangular and multisine inputs. It can be seen that, for both references, the PI controller with feedforward results in significantly smaller tracking error. We have further conducted comparison of the two PI controllers for sinusoidal references across the frequency range of 1–200 Hz. These results are reported in Table 2 and visualized in Fig. 17, which again confirm the effectiveness of including the feedforward component.

5 Conclusion

In this paper, we analyzed a closed-loop system involving hysteresis inversion, proportional-integral feedback control, and a constant-gain feedforward element. Some researchers in the literature use optimization [21], neural networks [33], or trial-and-error to determine both k_i and k_p. Depending on the uncertainties on the operator parameters, in this paper we found some criteria for determining the choice of those gains. For instance, the ratio k_i/k_p should be high to guarantee good performance, which agrees with the results in Refs. [21,33]. Singular perturbation analysis was used in order to separate fast dynamics of the plant from slow dynamics of the controller. The analysis quantifies the effect of the reference frequency on the tracking performance, which is important in applications such as high-speed nanopositioning. Simulation results were compared with the analytical expressions. The agreement between the simulation and analytical results provides support for the proposed analysis approach. Experimental results further strengthen the validity of the analysis. We note that, while simulation could provide a more accurate answer than the analytical approximation for a specific set of system parameters and a particular reference input, it does not provide direct insight into how the parameters determine the behavior of the tracking error, and consequently, has limited use in guiding the system and control design. On the contrary, the analysis presented in this paper offers general insight into the system behavior and guidance on controller design without running excessive simulations.

The presented singular perturbation analysis hinges on the assumption that the plant dynamics is much faster than the operating frequency range. If the closed-loop system operates close to the bandwidth of the plant dynamics, the accuracy of the singular perturbation analysis will be comprised. In practice, however, the gains of the PI controller are limited by stability concerns and cannot be increased freely to achieve an arbitrarily high bandwidth. The concern of device safety also places limits on the operating frequency; for example, the manufacturer of the nanopositioner used in this paper cautions against operating the device higher than 200 Hz (about one-tenth of the first-mode resonant frequency), to avoid excessive vibration and subsequent damage to the device. Therefore, the assumption of the plant dynamics being much faster than the controller states is valid for most operational scenarios.

The proportional-integral control was chosen in this paper due to its wide use and simplicity, and the latter facilitates the presentation of the proposed singular perturbation analysis. In future work, we will extend the current analysis to other higher-order controllers (e.g., the sliding mode controller) and more complicated systems. We will also quantify the impact of the parameters and their uncertainties for several important hysteresis operators, such as the (modified) PI operator and Preisach-Kransnoselskii-Porkovskii (PKP) operator, on the tracking performance.

Appendix A: Solution of ξ_0

In order to see how the solution develops and the error propagates from one hysteresis segment to another, we solve the equations for each segment by dividing the time into intervals that correspond to the time periods of the hysteresis staying in different segments. The solution of Eq. (21) for $t_i \le t < t_{i+1}$ is

$$\xi_0(t) = e^{A_{0i}(t-t_i)}\xi_0(t_i) + \int_{t_i}^{t} e^{A_{0i}(t-\tau)}(B_{0i}A_c\sin(\omega\tau) - H_i\gamma_i')d\tau \tag{A1}$$

which can be readily derived as

$$\begin{aligned}\xi_0(t) = {} & e^{A_{0i}(t-t_i)}\xi_0(t_i) + \frac{H_i\gamma_i'}{A_{0i}}[1 - e^{A_{0i}(t-t_i)}] \\ & - e^{A_{0i}(t-t_i)}B_{0i}A_c\left[\frac{-A_{0i}}{A_{0i}^2+\omega^2}\sin(\omega t_i) - \frac{\omega}{A_{0i}^2+\omega^2}\cos(\omega t_i)\right] \\ & + B_{0i}A_c\left[\frac{-A_{0i}}{A_{0i}^2+\omega^2}\sin(\omega t) - \frac{\omega}{A_{0i}^2+\omega^2}\cos(\omega t)\right]\end{aligned} \tag{A2}$$

With the assumption that the solution is periodic, we solve ξ_0 by starting at one segment i and continue solving for all n segments until we return back to segment i after a period T. At time $t = t_{i+1}$, Eq. (A2) becomes

$$\begin{aligned}\xi_0(t_{i+1}) = {} & e^{A_{0i}(t_{i+1}-t_i)}\xi_0(t_i) + \frac{H_i\gamma_i'}{A_{0i}}[1 - e^{A_{0i}(t_{i+1}-t_i)}] \\ & - e^{A_{0i}(t_{i+1}-t_i)}B_{0i}A_c\left[\frac{-A_{0i}}{A_{0i}^2+\omega^2}\sin(\omega t_i)\right. \\ & \left. - \frac{\omega}{A_{0i}^2+\omega^2}\cos(\omega t_i)\right] + B_{0i}A_c\left[\frac{-A_{0i}}{A_{0i}^2+\omega^2}\sin(\omega t_{i+1})\right. \\ & \left. - \frac{\omega}{A_{0i}^2+\omega^2}\cos(\omega t_{i+1})\right]\end{aligned} \tag{A3}$$

It is straightforward to use recursion to obtain $\xi_0(t_{n+i})$. Because the solution is periodic, we can set up the equation $\xi_0(t_{n+i}) = \xi_0(t_i)$ to solve for $\xi_0(t_i)$. More details can be found in Ref. [32]. Then by inserting $\xi_0(t_i)$, we obtain the solution of $\xi_0(t)$ at the steady state as

$$\xi_0(t) = \varphi + \frac{H_i\gamma_i'}{A_{0i}} + B_{0i}A_c\left(\frac{-A_{0i}}{A_{0i}^2+\omega^2}\sin(\omega t) - \frac{\omega}{A_{0i}^2+\omega^2}\cos(\omega t)\right) \tag{A4}$$

where φ is the periodic decaying term in the form of Eq. (24), the complete expression of which can be found in Ref. [32].

Appendix B: Solution for ξ_1

To solve for ξ_1, insert ξ_0 from Eq. (A4) into Eq. (22)

$$\begin{aligned}\dot{\xi}_1 = {} & A_{0i}\xi_1 - HLA_{0i}\left[\varphi - \frac{H_i\gamma_i'}{A_{0i}} + B_{0i}A_c\left(\frac{A_{0i}}{A_{0i}^2+\omega^2}\sin(\omega t)\right.\right. \\ & \left.\left. - \frac{\omega}{A_{0i}^2+\omega^2}\cos(\omega t)\right)\right] + [-HLA_{12}W - B_1HL]A_c\sin(\omega t) \\ & + HWA_c\omega\cos(\omega t)\end{aligned} \tag{B1}$$

By combining similar terms, we can rewrite Eq. (B1) as:

$$\dot{\xi}_1 = A_0\xi_1 + \alpha_1\sin(\omega t) + \alpha_2\cos(\omega t) + \alpha_3\omega\cos(\omega t) + Q \tag{B2}$$

where Q is a constant and α_1, α_2, and α_3 are bounded uniformly in ω. We notice form (B2) that $\dot{\xi}_1$ has the same form as $\dot{\xi}_0$ of Eq. (21) except with an extra term which comes from $\dot{y}_r$ and is proportional to the frequency ω. Since ξ_1 in the solution of the error will be multiplied by ε, it matters in determining the bound only if any terms of its solution can be approximated by a quantity that is proportional to ω. However, through similar derivation as for ξ_0, we will have a solution to ξ_1 with extra terms of sine and cosine terms multiplied by ω. These terms appear as follows:

$$\alpha_3\omega\left(\frac{\omega}{A_{0i}^2+\omega^2}\sin(\omega t) + \frac{A_{0i}}{A_{0i}^2+\omega^2}\cos(\omega t)\right)$$

which are bounded by a constant independent of the frequency and hence belong to the e_ε terms of Eq. (29).

Appendix C: Fast Variable Analysis

Now we need to express the fast variable η using its model (19) by finding $O(1)$ and $O(\varepsilon)$ terms.

Let us simplify Eq. (19) as

$$\varepsilon\dot{\eta} = A_{\eta_i}\eta + B_{\eta_i}y_r + \gamma_i' - \varepsilon W\dot{y}_r \tag{C1}$$

where $A_\eta = (A_{22} + \varepsilon LA_{12}), B_\eta = B_2 + \varepsilon LB_1 + (A_{22} + \varepsilon LA_{12})W)$. The solution of (C1) for $t_i \le t < t_{i+1}$ is

$$\begin{aligned}\eta(t) = {} & e^{A_{\eta_i}(t-t_i)/\varepsilon}\eta(t_i) + \frac{1}{\varepsilon}\int_{t_i}^{t} e^{A_{\eta_i}(t-\tau)/\varepsilon}[B_{\eta_i}y_r + \gamma_i' - \varepsilon W\dot{y}_r(\tau)]d\tau \\ = {} & e^{A_{\eta_i}(t-t_i)/\varepsilon}\eta(t_i) - A_{\eta_i}^{-1}e^{A_{\eta_i}(t-\tau)/\varepsilon}\big|_{t_i}^{t}\gamma_i' \\ & + \frac{1}{\varepsilon}\int_{t_i}^{t} e^{A_{\eta_i}(t-\tau)/\varepsilon}B_{\eta_i}y_r(\tau)d\tau - \int_{t_i}^{t} e^{A_{\eta_i}(t-\tau)/\varepsilon}W\dot{y}_r(\tau)d\tau\end{aligned} \tag{C2}$$

The details of solving Eq. (C2) are given in Ref. [32]. We arrive at

$$\begin{aligned}\eta(t) = {} & e^{A_{\eta_i}(t-t_i)/\varepsilon}\left(\eta(t_i) + A_{\eta_i}^{-1}\gamma_i' + A_{\eta_i}^{-1}B_{\eta_i}y_r(t_i)\right. \\ & \left. + \varepsilon A_{\eta_i}^{-2}B_{\eta_i}\dot{y}_r(t_i) - \varepsilon A_{\eta_i}^{-1}W\dot{y}_r(t_i) - A_{\eta_i}^{-1}\gamma_i'\right) - A_{\eta_i}^{-1}B_{\eta_i}y_r(t) \\ & + \varepsilon A_{\eta_i}^{-1}W\dot{y}_r(t) - \varepsilon A_{\eta_i}^{-2}B_{\eta_i}\dot{y}_r(t) + O(\varepsilon^2)\end{aligned} \tag{C3}$$

To obtain the initial value $\eta(t_i)$, we do not need to solve (C3) by getting the accumulation around one cycle because we assume ε is small and the decaying within each segments makes the transients the order of $O(\varepsilon)$. Thus, the initial value of the current segment, $i=i+n$, only depends on the driving terms of the previous segment, $i+n-1$.

$$\begin{aligned}\eta(t_i) = e^{A_{\eta_{i+n-1}}(t_i-t_{i+n-1})/\varepsilon}\Big(&\eta(t_{i+n-1}) + A^{-1}_{\eta_{i+n-1}}\gamma'_{i+n-1} \\ &+ A^{-1}_{\eta_{i+n-1}}B_{\eta_{i+n-1}}y_r(t_{i+n-1}) + \varepsilon A^{-2}_{\eta_{i+n-1}}B_{\eta_{i+n-1}}\dot{y}_r(t_{i+n-1}) \\ &-\varepsilon A^{-1}_{\eta_{i+n-1}}W\dot{y}_r(t_{i+n-1})\Big) - A^{-1}_{\eta_{i+n-1}}\gamma'_{i+n-1} \\ &- A^{-1}_{\eta_{i+n-1}}B_{\eta_{i+n-1}}y_r(t_i) - \varepsilon A^{-2}_{\eta_{i+n-1}}B_{\eta_{i+n-1}}\dot{y}_r(t_i) \\ &+ \varepsilon A^{-1}_{\eta_{i+n-1}}W\dot{y}_r(t_i) + O(\varepsilon^2)\end{aligned} \tag{C4}$$

Now by ignoring the term in the parenthesis in Eq. (C4) and substituting the remaining term of $\eta(t_i)$ into (C3), we obtain

$$\begin{aligned}\eta(t) = \psi - A^{-1}_{\eta_i}\gamma'_i - A^{-1}_{\eta_i}B_{\eta_i}y_r(t) + \varepsilon A^{-1}_{\eta_i}W\dot{y}_r(t) \\ - \varepsilon A^{-2}_{\eta_i}B_{\eta_i}\dot{y}_r(t) + O(\varepsilon^2)\end{aligned} \tag{C5}$$

where

$$\begin{aligned}\psi = e^{A_{\eta_i}(t-t_i)/\varepsilon}\Big(&-A^{-1}_{\eta_{i+n-1}}\gamma'_{i+n-1} - A^{-1}_{\eta_{i+n-1}}B_{\eta_{i+n-1}}y_r(t_i) \\ &+ \varepsilon A^{-1}_{\eta_{i+n-1}}W\dot{y}_r(t_i) - \varepsilon A^{-2}_{\eta_{i+n-1}}B_{\eta_{i+n-1}}\dot{y}_r(t_i) + A^{-1}_{\eta_i}\gamma'_i \\ &+ A^{-1}_{\eta_i}B_{\eta_i}y_r(t_i) - \varepsilon A^{-1}_{\eta_i}W\dot{y}_r(t_i) + \varepsilon A^{-2}_{\eta_i}B_{\eta_i}\dot{y}(t_i)\Big)\end{aligned} \tag{C6}$$

The term ψ is bounded for the following reasons. First, the highest value happens at the beginning of each segment i, $t=t_i$, which makes the exponential term equal to one. Second, with the assumption $|\Delta_m| < m$, the terms which are functions of y_r or $\dot{y}_r$ cancel out because every term has a similar term with opposite sign and close to it in value. The contribution of the remaining terms, $A^{-1}_{\eta_i}\gamma'_i - A^{-1}_{\eta_{i+n-1}}\gamma'_{i+n-1}$, to the tracking error is calculated by multiplying it by A_{12}. This results in $H_i\gamma'_i - H_{i+n-1}\gamma'_{i+n-1}$. By inserting the matrix expressions in $H_i\gamma'_i$, we obtain

$$\begin{aligned}H_i\gamma'_i &= -C\left[A - k_p\frac{m_i+\Delta_{m_i}}{m_i}BC\right]^{-1}B\left(\frac{m_i\Delta_{\gamma_i} - \gamma_i\Delta_{m_i}}{m_i}\right) \\ &= \frac{-h(m_i\Delta_{\gamma_i} - \gamma_i\Delta_{m_i})}{1+k_p(m_i+\Delta_{m_i})h}\end{aligned} \tag{C7}$$

Using $y_r = A_c\sin(\omega t)$ in Eq. (26) and including the subscript i for the parameters, we have the expression of η for the time from t_i to t_{i+1} as

$$\begin{aligned}\eta = \psi - A^{-1}_{\eta,i}B_{\eta,i}A_c\sin(\omega t) - A^{-1}_{\eta,i}\gamma' \\ + \varepsilon(A^{-1}_{\eta,i}W - A^{-2}_{\eta,i}B_{\eta,i})A_c\omega\cos(\omega t) + O(\varepsilon^2)\end{aligned} \tag{C8}$$

Appendix D: Calculating the Bound on the Frequency-Dependent Term of the Error

To determine the upper bound on the third term $\varepsilon(H_iA^{-1}_{22,i}B_{2,i})\omega A_c$ of Eq. (35), we replace H_i by $A_{12}A^{-1}_{22,i}$ and $B_{2,i}$ by $B\beta_2$, where $\beta_2 = ((m_i+\Delta_{m_i})/m_i)(g+k_p)$. We also replace $A^{-1}_{22,i}$ by $A - B\beta_1C$, where $\beta_1 = ((m_i+\Delta_{m_i})/m_i)k_p$ and simplify the expressions

$$\begin{aligned}H_iA^{-1}_{22,i}B_{2,i} &= A_{12}A^{-2}_{22,i}B_{2,i} \\ &= -\Bigg[CA^{-2}B + CA^{-2}(BC)^2A^{-2}B\left(\frac{\beta_1}{1+h\beta_1}\right)^2 \\ &\quad + 2CA^{-2}B\left(\frac{\beta_1}{1+h\beta_1}\right)CA^{-1}B\Bigg]\beta_2\end{aligned} \tag{D1}$$

Because C is a row vector and B is a column vector, the multiplications of all the matrices in (D1) are scalar quantities. Let us denote them by q_1, q_2, and q_3 and replace β_1 and β_2 by their expressions.

$$\begin{aligned}H_iA^{-1}_{22,i}B_{2,i} = -\Bigg[&q_1 + q_2\left(\frac{(m_i+\Delta_{m_i})k_p}{m_i + k_p(m_i+\Delta_{m_i})h}\right)^2 \\ &+ q_3\left(\frac{(m_i+\Delta_{m_i})k_p}{m_i + k_p(m_i+\Delta_{m_i})h}\right)\Bigg]\frac{m_i+\Delta_{m_i}}{m_i}(g+k_p)\end{aligned} \tag{D2}$$

Let us denote the bound on $H_iA^{-1}_{22,i}B_{2,i}$ By $(HA^{-1}_{22}B_2)_{\max}$ for all segments. This is obtained by substituting the largest slope $m_{\max}$ and uncertainty $|\Delta_m|_{\max}$ in the numerator and the smallest $m_{\min}$ in the denominator of Eq. (D2)

$$\begin{aligned}(HA^{-1}_{22}B_2)_{\max} = &-\frac{m_{\max}+|\Delta_m|_{\max}}{m_{\min}}(g+k_p) \\ &+ \Bigg[q_1q_2\left(\frac{(m_{\max}+|\Delta_m|_{\max})k_p}{m_{\min}(1+k_ph)}\right)^2 \\ &+ q_3\left(\frac{(m_{\max}+|\Delta_m|_{\max})k_p}{m_{\min}(1+k_ph)}\right)\Bigg]\end{aligned} \tag{D3}$$

We notice from Eq. (D2), in the case when $|\Delta_{m_i}| \ll m_i$ such that we can ignore $|\Delta_{m_i}|$, Eq. (D2) becomes independent of the slopes and uncertainties. In this case, the term of $H_iA^{-1}_{22,i}B_{2,i}$ becomes constant through all the segments.

References

[1] Devasia, S., Eleftheriou, E., and Moheimani, S. O., 2007, "A Survey of Control Issues in Nanopositioning," IEEE Trans. Control Syst. Technol., **15**(5), pp. 802–823.

[2] Yong, Y. K., Aphale, S. S., and Moheimani, S. R., 2009, "Design, Identification, and Control of a Flexure-Based XY Stage for Fast Nanoscale Positioning," IEEE Trans. Nanotechnol., **8**(1), pp. 46–54.

[3] Kuhnen, K., and Janocha, H., 2001, "Inverse Feedforward Controller for Complex Hysteretic Nonlinearities in Smart-Material Systems," Control Intell. Syst., **29**(3), pp. 74–83.

[4] Janaideh, M. A., Rakheja, S., and Su, C.-Y., 2011, "An Analytical Generalized Prandtlishlinskii Model Inversion for Hysteresis Compensation in Micropositioning Control," IEEE/ASME Trans. Mechatronics, **16**(4), pp. 734–744.

[5] Mayergoyz, I., 1986, "Mathematical Models of Hysteresis," IEEE Trans. Magn., **22**(5), pp. 603–608.

[6] Kuhnen, K., 2003, "Modeling, Identification, and Compensation of Complex Hysteretic Nonlinearities—A Modified Prandtl-Ishlinskii Approach," Eur. J. Control, **9**(4), pp. 407–418.

[7] Tao, G., and Kokotovic, P., 1995, "Adaptive Control of Plants With Unknown Hysteresis," IEEE Trans. Autom. Control, **40**(2), pp. 200–212.

[8] Croft, D., Shedd, G., and Devasia, S., 2000, "Creep, Hysteresis, and Vibration Compensation for Piezo Actuators: Atomic Force Microscopy Application," Proceedings of the 2000 American Control Conference, pp. 2123–2128.

[9] Iyer, R., and Tan, X., 2009, "Control of Hysteretic Systems Through Inverse Compensation: Inversion Algorithms, Adaptation, and Embedded Implementation," IEEE Control Syst Mag., **29**(1), pp. 83–99.

[10] Chen, X., Hisayama, T., and Su, C.-Y., 2008, "Pseudo-Inverse-Based Adaptive Control for Uncertain Discrete Time Systems Preceded by Hysteresis," Automatica, **45**, pp. 469–476.

[11] Tan, X., and Baras, J. S., 2004, "Modeling and Control of Hysteresis in Magnetostrictive Actuators," Automatica, **40**(9), pp. 1469–1480.

[12] Tan, X., and Baras, J., 2005, "Adaptive Identification and Control of Hysteresis in Smart Materials," IEEE Trans. Autom. Control, **50**(6), pp. 827–839.

[13] Tan, X., and Khalil, H. K., 2009, "Two-Time-Scale Averaging of Systems Involving Operators and Its Application to Adaptive Control of Hysteretic Systems," Proceedings of the 2009 American Control Conference, pp. 4476–4481.

[14] Esbrook, A., Tan, X., and Khalil, H. K., 2013, "Control of Systems With Hysteresis Via Servocompensation and Its Application to Nanopositioning," IEEE Trans. Control Syst. Technol., **21**(3), pp. 725–738.
[15] Kuhnen, K., and Janocha, K., 1999, "Adaptive Inverse Control of Piezoelectric Actuators With Hysteresis Operator," Proceedings of the European Control Conference, Germany, Paper F 0291.
[16] Shen, J., Jywea, W., Chiang, H., and Shub, Y., 2008, "Precision Tracking Control of a Piezoelectric-Actuated System," Precis. Eng., **32**, pp. 71–78.
[17] Bashash, S., and Jalili, N., 2007, "Robust Multiple Frequency Trajectory Tracking Control of Piezoelectrically Driven Micro/Nanopositioning Systems," IEEE Trans. Control Syst. Technol., **15**(5), pp. 867–878.
[18] Su, C. Y., Stepanenko, Y., Svoboda, J., and Leung, T. P., 2000, "Robust Adaptive Control of a Class of Nonlinear Systems With Unknown Backlash-Like Hysteresis," IEEE Trans. Autom. Control, **45**, pp. 2427–2432.
[19] Bashash, S., and Jalili, N., 2009, "Robust Adaptive Control of Coupled Parallel Piezo-Flexural Nanopositioning Stages," IEEE/ASME Trans. Mechatronics, **14**, pp. 11–20.
[20] Zhong, J., and Yao, B., 2008, "Adaptive Robust Precision Motion Control of a Piezoelectric Positioning Stage," IEEE Trans. Control Syst. Technol., **16**, pp. 1039–1046.
[21] Valadkhan, S., Morris, K., and Khajepour, A., 2008, "Robust PI Control of Hysteretic Systems," Proceedings of the 47th IEEE Conference on Decision and Control, pp. 3787–3792.
[22] Wu, Y., and Zou, Q., 2007, "Iterative Control Approach to Compensate for Both the Hysteresis and the Dynamics Effects of Piezo Actuators," IEEE Trans. Control Syst. Technol., **15**(5), pp. 936–944.
[23] Ge, P., and Jouaneh, M., 1996, "Tracking Control of a Piezoceramic Actuator," IEEE Trans. Control Syst. Technol., **4**(3), pp. 209–216.
[24] Prempain, E., and Postlethwaite, I., 2001, "Feedforward Control: A Full-Information Approach," Automatica, **37**(1), pp. 17–28.
[25] Youla, D., and Bongiorno, J., 1985, "A Feedback Theory of Two-Degree-of-Freedom Optimal Wiener-Hopf Design," IEEE Trans. Autom. Control, **30**(7), pp. 652–665.
[26] Howze, J., and Bhattacharyya, S., 1997, "Robust Tracking, Error Feedback, and Two-Degree-of-Freedom Controllers," IEEE Trans. Autom. Control, **42**(7), pp. 990–983.
[27] Hara, S., and Sugie, T., 1988, "Independent Parameterization of Two-Degree-of-Freedom Compensators in General Robust Tracking Systems," IEEE Trans. Autom. Control, **33**(1), pp. 59–67.
[28] Edardar, M., Tan, X., and Khalil, H. K., 2012, "Tracking Error Analysis for Singularly Perturbed Systems Preceded by Piecewise Linear Hysteresis," Proceedings of the 51th IEEE Conference on Decision and Control, pp. 3139–3144.
[29] Zhou, K., and Doyk, J., 1998, *Essentials of Robust Control*, Tom Robbins, Upper Saddle River, NJ.
[30] Khalil, H., 2002, *Nonlinear Systems*, Prentice-Hall, Englewood Cliffs, NJ.
[31] Kokotovic, P., Khalil, H. K., and O'reilly, J., 1999, "*Singular Perturbation Methods in Control Analysis*," SIAM, Philadelphia, PA.
[32] Edardar, M., 2013, "Robust Control of Systems With Piecewise Linear Hysteresis," Ph.D. thesis, Michigan State University, East Lansing, MI.
[33] Wei, Q., Hu, C., and Zhang, D., 2010, "Precision Control of Piezoelectric Actuated Mechanism in Scanning Tunneling Microscope," Proceedings of the 8th World Congress on Intelligent Control and Automation (WCICA), pp. 1262–1267.